BRIEF DEFINITIVE REPORT

The mRNA m⁶A reader YTHDF2 suppresses proinflammatory pathways and sustains hematopoietic stem cell function

Christopher Mapperley[1,2] ●, Louie N. van de Lagemaat[1,2]* ●, Hannah Lawson[2]* ●, Andrea Tavosanis[2]* ●, Jasmin Paris[1,2] ●, Joana Campos[2] ●, David Wotherspoon[2] ●, Jozef Durko[2] ●, Annika Sarapuu[2] ●, Junho Choe[3,4] ●, Ivayla Ivanova[1,8] ●, Daniela S. Krause[5] ●, Alex von Kriegsheim[6] ●, Christian Much[1,8] ●, Marcos Morgan[1,8] ●, Richard I. Gregory[3,4] ●, Adam J. Mead[7] ●, Dónal O'Carroll[1,8,9]** ●, and Kamil R. Kranc[1,2]** ●

The mRNA *N*⁶-methyladenosine (m⁶A) modification has emerged as an essential regulator of normal and malignant hematopoiesis. Inactivation of the m⁶A mRNA reader YTHDF2, which recognizes m⁶A-modified transcripts to promote m⁶A-mRNA degradation, results in hematopoietic stem cell (HSC) expansion and compromises acute myeloid leukemia. Here we investigate the long-term impact of YTHDF2 deletion on HSC maintenance and multilineage hematopoiesis. We demonstrate that *Ythdf2*-deficient HSCs from young mice fail upon serial transplantation, display increased abundance of multiple m⁶A-modified inflammation-related transcripts, and chronically activate proinflammatory pathways. Consistent with the detrimental consequences of chronic activation of inflammatory pathways in HSCs, hematopoiesis-specific *Ythdf2* deficiency results in a progressive myeloid bias, loss of lymphoid potential, HSC expansion, and failure of aged *Ythdf2*-deficient HSCs to reconstitute multilineage hematopoiesis. Experimentally induced inflammation increases YTHDF2 expression, and YTHDF2 is required to protect HSCs from this insult. Thus, our study positions YTHDF2 as a repressor of inflammatory pathways in HSCs and highlights the significance of m⁶A in long-term HSC maintenance.

Introduction

Emerging evidence indicates the importance of the mRNA *N*⁶-methyladenosine (m⁶A) modification in hematopoietic stem cell (HSC) biology and leukemic transformation (Vu et al., 2019). m⁶A is the most abundant internal mRNA modification, which is cotranscriptionally installed by the "m⁶A writer" complex, consisting of the METTL3/METTL14 enzymatic core and their regulator WT-associated protein (Frye et al., 2018). The modification can be reversed by m⁶A demethylases (FTO and AlkBH5), collectively called "m⁶A erasers." m⁶A-modified transcripts are recognized by "m⁶A readers," including nuclear YTHDC1 (YTH domain-containing 1) and cytoplasmic YTH domain-containing family member 1 (YTHDF1), YTHDF2, YTHDF3, and YTHDC2, which execute the outcome of m⁶A modification by promoting splicing, nuclear export, translation, or degradation. Recent studies

demonstrated that loss of METTL3, METTL14, or FTO weakens acute myeloid leukemia (AML) propagation, whereas inactivation of METTL3 and METTL14 has deleterious consequences for normal HSC maintenance (Barbieri et al., 2017; Cheng et al., 2019; Li et al., 2017; Vu et al., 2017; Weng et al., 2018). Furthermore, inactivation of YTHDF2, which recognizes m⁶A-modified mRNA to mediate m⁶A-mRNA degradation (Du et al., 2016; Wang et al., 2015), compromises initiation and propagation of AML and results in HSC expansion (Li et al., 2018; Paris et al., 2019; Wang et al., 2018). However, the involvement of m⁶A or its readers in long-term HSC maintenance upon aging remains unknown. Here, we reveal that YTHDF2 functions to down-regulate m⁶A modified transcripts involved in the inflammatory response and maintains HSC integrity upon aging.

Results and discussion

YTHDF2-deficient HSCs activate proinflammatory pathways and lose their reconstitution capacity upon serial transplantation

We have recently demonstrated that hematopoiesis-specific *Vav-iCre*–mediated deletion of *Ythdf2* results in HSC expansion and compromises AML initiation and propagation (Paris et al., 2019). We used the conditional and reporter *Ythdf2*fl mouse allele in which exon 2 of *Ythdf2* was flanked by *loxP* sites and GFP was introduced after the start codon of *Ythdf2*, generating a fully functional GFP-YTHDF2 fusion protein (Ivanova et al., 2017). Our published data indicated that 8–12-wk-old *Ythdf2*fl/fl;*Vav-iCre* (conditional knockout, *Ythdf2*CKO) mice displayed largely unaffected hematopoiesis compared with control *Ythdf2*fl/fl (control, *Ythdf2*CTL) mice, with modest decreases in numbers of white and red blood cells, B cells, and CD8+ T cells (Paris et al., 2019). Furthermore, while HSCs from 8–12-wk-old *Ythdf2*CKO mice displayed myeloid bias upon primary transplantation and robustly contribute to the bone marrow (BM) HSC and progenitor cell compartments (Paris et al., 2019), the role of YTDHF2 in long-term HSC maintenance remains unknown. To address this, we performed secondary transplantation assays by sorting CD45.2+ Lin−c-Kit+Sca-1+ (LSK) cells from primary recipients of *Ythdf2*CKO and *Ythdf2*CTL HSCs (Paris et al., 2019) and retransplanting them (together with supporting BM cells) into lethally irradiated secondary recipient mice (Fig. 1 A). Strikingly, *Ythdf2*CKO HSCs failed to efficiently repopulate long-term multilineage hematopoiesis and stem and progenitor cell compartments in secondary recipients (Fig. 1, B–D) and displayed myeloid bias (Fig. S1 A). Thus, HSCs critically require YTHDF2 to sustain their function upon serial transplantation.

To understand the cause of the failure of *Ythdf2*-deficient HSCs upon serial transplantation, we next set out to determine the molecular signature of *Ythdf2*-deficient HSCs. *Ythdf2* deficiency resulted in deregulated gene expression (Fig. 1 E), with 81 up-regulated transcripts and 33 down-regulated transcripts (false discovery rate [FDR] < 0.05) in *Ythdf2*CKO compared with *Ythdf2*CTL HSCs. Strikingly, gene set enrichment analysis (GSEA) on *Ythdf2*CKO versus *Ythdf2*CTL HSCs revealed significant up-regulation of numerous inflammation-related processes, such as IFN-α response, IFN-γ response, inflammatory response, TNF-α signaling, and IL6/JAK/STAT3 signaling (Fig. 1 F and Fig. S1 B).

Given that proinflammatory signals are known to drive overproliferation of HSCs, ultimately resulting in loss of HSC function (Essers et al., 2009; Pietras, 2017), we aimed to confirm the proinflammatory signature in *Ythdf2*-deficient HSCs using additional approaches. We found that HSCs from *Ythdf2*CKO mice displayed increased expression of cell surface Sca-1 protein (Fig. 1 G), which is used as a proxy of IFN signaling (Essers et al., 2009). Furthermore, *Ythdf2*-deficient HSCs showed elevated levels of phosphorylated forms of STAT1 and STAT3 proteins, key mediators of IFN signaling (Fig. 1 H).

Given that *Ythdf2*-deficient HSCs showed up-regulation of proinflammatory pathways and displayed a myeloid bias (a hallmark of inflammation), we aimed to determine whether the primitive progenitor comp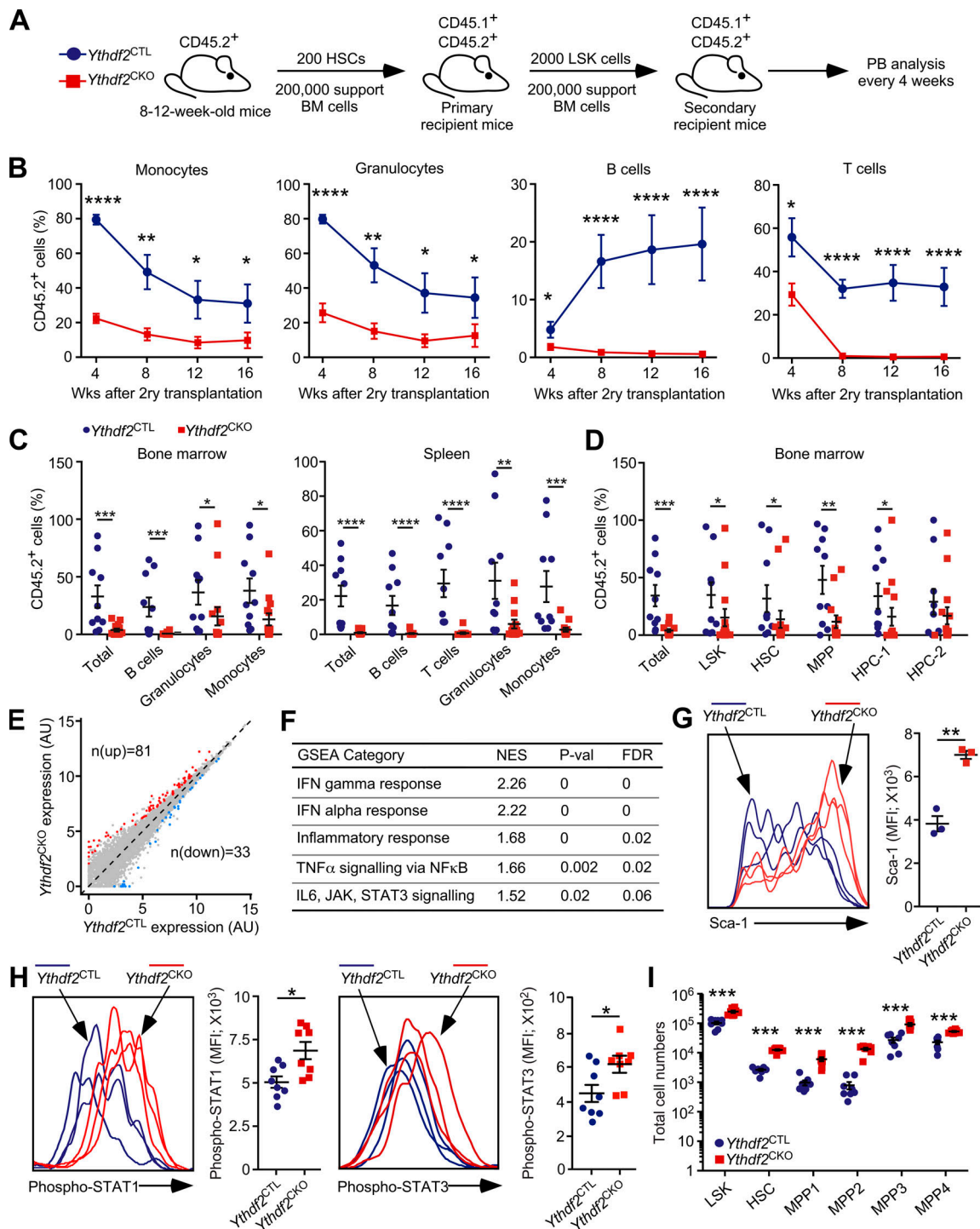artment also reflected innate immune activation in *Ythdf2*CKO mice. During steady-state normal hematopoiesis, HSCs generate functionally distinct lineage-biased multipotent progenitors (MPPs), with MPP2/3 and MPP4 populations predominantly sustaining myeloid and lymphoid lineages, respectively (Pietras et al., 2015). Stressful conditions such as infection, stress, or injury induce proinflammatory stimuli, which not only activate HSCs but also cause expansion of MPPs, in particular myeloid-biased MPP2/3 populations, thereby driving myeloid differentiation at the expense of HSC integrity (Essers et al., 2009; Pietras et al., 2016; Yamashita and Passegue, 2019; Zhang et al., 2017; Zhang et al., 2016). Consistent with the activation of proinflammatory pathways, we found that 8–12-wk-old *Ythdf2*CKO mice displayed expansion of HSCs and a concurrent increase in all four main subpopulations, namely MPP1-4 cells (Fig. 1 I). Thus, hematopoietic-specific deletion of *Ythdf2* results in a constitutive up-regulation of the proinflammatory signature, expansion of HSCs and MPPs, and a failure of HSC function upon serial transplantation.

YTHDF2 functions to suppress m⁶A-modified proinflammatory transcripts

YTHDF2 regulates the transcriptome by binding m⁶A modified transcripts to promote their decay through deadenylation (Du et al., 2016; Wang et al., 2014). To identify YTHDF2 target transcripts, we aimed to determine mRNAs that were methylated in normal conditions and up-regulated in *Ythdf2*CKO HSCs. m⁶A sequencing (m⁶A-seq) in c-Kit+ hematopoietic stem and progenitor cells was used to determine transcriptome-wide m⁶A distribution. This identified the expected distribution of m⁶A within the transcriptome (i.e., enrichment around the stop codons; Fig. 2, A and B) as well as the m⁶A consensus motif (DRACH; D = A, G, or U; R = purine; and H = A, C, or U; Fig. 2 C). Consistent with the role of YTHDF2 in promoting degradation of m⁶A-modified transcripts, we found that transcripts that contain m⁶A modification ($P = 2.6 \times 10^{-40}$, 8,253 genes) show increased expression in *Ythdf2*CKO HSCs (Fig. 2 D). Ingenuity pathway analysis (IPA) indicated that up-regulated genes are enriched for transcripts related to inflammatory responses (including IFN-γ, TNF-α, IFN-α, IFN regulatory factor 7, STAT1, and TLR4; Fig. 2 E and Fig. S2 A). Importantly, m⁶A-seq revealed that a large proportion of these key up-regulated transcripts in HSCs are m⁶A modified, including key genes involved in inflammation such as *Stat1*, *Il6ra*, and *Gadd45g* (Fig. 2, E and F).

The up-regulation of m⁶A-modified transcripts involved in inflammation upon loss of YTHDF2 may be a consequence of an increase in their half-life. Given that the measurement of transcript half-life in HSCs is technically not possible, to address this, we analyzed our SLAM-seq dataset from immortalized c-Kit+ cells derived from *Ythdf2*CTL and *Ythdf2*CKO mice (Paris et al., 2019), which allowed us to measure the transcriptome-wide mRNA half-life (Herzog et al., 2017). We found that multiple m⁶A-modified transcripts that are up-regulated upon *Ythdf2* deletion (Fig. 2 E) also have their half-lives increased in the absence of *Ythdf2* (Fig. S2 B).

Finally, we next asked whether up-regulation of m⁶A-modified transcripts upon *Ythdf2* deletion corresponds to an increase in their protein level. Mass spectrometry can be used to obtain

Mapperley et al.
YTHDF2 suppresses inflammation to sustain HSCs

Journal of Experimental Medicine 2 of 11
https://doi.org/10.1084/jem.20200829

Figure 1. **HSCs lacking *Ythdf2* are expanded, activate proinflammatory pathways and prematurely lose function upon serial transplantation.**
(A) Experimental design. 200 BM LSK CD48⁻CD150⁺CD45.2⁺ HSCs from 8-wk-old *Ythdf2*^CKO and *Ythdf2*^CTL mice were transplanted to lethally irradiated syngeneic CD45.1⁺/CD45.2⁺ primary recipient mice together with 2 × 10⁵ competitor CD45.1⁺ BM cells (Paris et al., 2019). After 16 wk, 2,000 CD45.2⁺LSK cells were sorted from primary recipient mice and transplanted into lethally irradiated syngeneic CD45.1⁺/CD45.2⁺ secondary recipient mice together with 2 × 10⁵ competitor CD45.1⁺ BM cells. PB of secondary recipient mice was analyzed every 4 wk, and hematopoietic compartments were analyzed 16 wk after transplantation. **(B)** Percentage of CD45.2⁺ cells in the PB CD11b⁺Gr-1⁻ monocyte, CD11b⁺Gr-1⁺ granulocyte, CD19⁺ B cell, and CD4⁺ and CD8⁺ T cell compartments of secondary recipient mice over 16 wk. Data represent mean ± SEM; *, P < 0.05; ****, P < 0.0001 (Mann–Whitney *U* test); at least two independent experiments were performed. **(C)** Percentage of CD45.2⁺ cells in the BM and spleen overall and in the monocyte, granulocyte, B cell, and T cell compartments of secondary recipient mice 16 wk after transplantation. Data represent mean ± SEM; *, P < 0.05; **, P < 0.01; ***, P < 0.001; ****, P < 0.0001 (Mann–Whitney *U* test); at least two independent experiments were performed. **(D)** Percentage of CD45.2⁺ cells in the BM of secondary recipients and in the LSK, LSK CD48⁻CD150⁺ HSC, LSK CD48⁻CD150⁻ MPP, LSK CD48⁺CD150⁻ HPC-1, and LSK CD48⁺CD150⁺ HPC-2 cell compartments of secondary recipient mice 16 wk after transplantation. Data represent mean ± SEM; *, P < 0.05; **, P < 0.01; ***, P < 0.001 (Mann–Whitney *U* test); at least two independent experiments were

performed. **(E)** Transcript expression scatterplot from *Ythdf2*^CKO and *Ythdf2*^CTL HSCs from 8–12-wk-old mice (*n* = 4). Significantly dysregulated transcripts are highlighted and counted (FDR < 0.05; log$_2$ fold change < 1.2). **(F)** GSEA showing up-regulated pathways in HSCs from 8–12-wk-old *Ythdf2*^CKO mice compared with HSCs from *Ythdf2*^CTL mice. **(G)** Histogram and median Sca-1 fluorescence intensity in LSK CD48⁻CD150⁺ HSCs from *Ythdf2*^CKO and *Ythdf2*^CTL mice determined by flow cytometry. Data represent mean ± SEM; **, P < 0.01 (Mann–Whitney *U* test); at least two independent experiments were performed. **(H)** Phospho-STAT1 and phospho-STAT3 levels in LSK cells determined by flow cytometry. Data represent mean ± SEM; *, P < 0.05 (Mann–Whitney *U* test); at least two independent experiments were performed. **(I)** Total numbers of LSK cells, HSCs (LSK CD34⁻CD135⁻CD150⁺CD48⁻), and MPP1 (also referred to as short-term HSCs; LSK CD34⁺CD135⁻CD150⁺CD48⁻), MPP2 (LSK CD34⁺CD135⁻CD150⁺CD48⁺), MPP3 (LSK CD34⁺CD135⁻CD150⁻CD48⁺), and MPP4 (LSK CD34⁺CD135⁺CD150⁻CD48⁺) cell populations in BM of 8–12-wk-old *Ythdf2*^CKO and *Ythdf2*^CTL mice. Data represent mean ± SEM; ***, P < 0.001 (Mann–Whitney *U* test); at least two independent experiments were performed. AU, arbitrary units; MFI, mean fluorescence intensity.

the comprehensive but incomplete quantitative measurement of the proteome. IPA of quantitative mass spectrometry–based proteomics of immortalized *Ythdf2*^CTL and *Ythdf2*^CKO c-Kit⁺ cells indicated that up-regulated proteins are related to the same inflammatory responses found in the transcriptomic data ([Fig. S2 A](#)). Strikingly, based on the coverage of the proteomics dataset, we found that protein level of STAT1, IFN-γ inducible protein 47, IFN-γ–induced GTPaseP, sterile α motif domain containing 9 like, immunity-related GTPase family M protein 1, and TNF receptor 2, whose corresponding transcripts were up-regulated and methylated upon *Ythdf2* deletion, were elevated in *Ythdf2*-deficient cells ([Fig. 2, G and H](#)). Thus, YTHDF2 suppresses m⁶A-modified mRNAs, which are involved in multiple proinflammatory pathways within HSCs. Given that *Ythdf2* deletion results in up-regulation of multiple m⁶A-modified transcripts in HSCs, future genetic rescue experiments will reveal their relative contributions to their failure upon serial transplantation.

Aged HSCs lacking *Ythdf2* undergo expansion and sustain steady-state hematopoiesis but fail to reconstitute multilineage hematopoiesis upon transplantation

Proinflammatory signals are known to drive overproliferation of HSCs, promote myeloid bias, and ultimately lead to the loss of HSC activity ([Essers et al., 2009](#); [Pietras, 2017](#)). Furthermore, proinflammatory pathways are up-regulated in aged HSCs, indicating their roles in stem cell aging ([Yamashita and Passegue, 2019](#)). We found that both young and aged HSCs expressed comparable levels of the YTHDF2 protein ([Fig. S3 A](#)). To investigate the functional significance of YTHDF2 in unperturbed long-term multilineage hematopoiesis and maintenance of the HSC pool over a long period of time, we aged *Ythdf2*^CKO and *Ythdf2*^CTL mice for 1 yr ([Fig. 3 A](#)). Analyses of 60–65-wk-old *Ythdf2*^CKO mice revealed increased numbers of peripheral blood (PB) granulocytes and monocytes (i.e., myeloid bias); however, hematopoiesis was otherwise largely unaffected ([Fig. 3, B and C](#); and [Fig. S3, B and C](#)). Furthermore, 60–65-wk-old *Ythdf2*^CKO mice displayed expansion of BM HSCs and primitive hematopoietic progenitor cell populations ([Fig. 3 D](#)). HSCs from these mice showed increased expression of Sca-1 ([Fig. 3 E](#)), indicating constitutive activation of proinflammatory signals. To test the ability of the expanded aged HSCs to reconstitute multilineage hematopoiesis, we competitively transplanted HSCs from 60–65-wk-old *Ythdf2*^CKO and *Ythdf2*^CTL mice into lethally irradiated recipients ([Fig. 3 A](#)). While HSCs from aged *Ythdf2*^CTL mice robustly repopulated both myeloid and lymphoid lineages, HSCs from aged *Ythdf2*^CKO mice failed to efficiently reconstitute short- and long-term multilineage hematopoiesis in the

recipients and displayed a myeloid bias ([Fig. 3 F](#) and [Fig. S1 C](#)). The contribution of *Ythdf2*-deficient HSCs to the HSC compartment of the recipients was also decreased compared with that of control HSCs ([Fig. 3 G](#)), albeit this was not as striking as their inability to reconstitute multilineage hematopoiesis ([Fig. 1 F](#)). Thus, while long-term *Ythdf2* deficiency in the hematopoietic system does not derail steady-state multilineage hematopoiesis, it devastates the multilineage reconstitution capacity of HSCs. Given that the inflammatory pathways affect multiple HSC fates ([Essers et al., 2009](#); [Pietras, 2017](#); [Pietras et al., 2014](#); [Pietras et al., 2016](#)), future investigations will be required to determine the exact impact of *Ythdf2* deletion on HSC survival, self-renewal, differentiation capacity, and homing.

Inducible *Ythdf2* deletion results in a progressive loss of lymphoid potential, with concurrent myeloid bias and subsequent HSC failure

To delete *Ythdf2* in adult mice in an inducible manner, we generated *Ythdf2*^iCKO mice in which *Ythdf2* can be ablated acutely in hematopoietic cells upon administration of polyinosinic-polycytidylic acid (pIpC). *Ythdf2*^iCKO and *Ythdf2*^CTL mice were treated with pIpC and analyzed 26 and 52 wk later ([Fig. 3 H](#)). Inducible *Ythdf2* deletion resulted in increased myeloid output ([Fig. S3, D–F](#)) and HSC expansion ([Fig. S3 G](#)), but multilineage hematopoiesis was otherwise largely unaffected ([Fig. S3, D–F](#)). Transplanted HSCs from mice 26 wk after *Ythdf2* deletion reconstituted myeloid lineages, failed to efficiently reconstitute lymphoid lineages ([Fig. 3 I](#) and [Fig. S1 D](#)), and contributed equally to the HSC compartment of recipients compared with control HSCs ([Fig. 3 J](#)). Strikingly, HSCs from mice 52 wk after *Ythdf2* ablation failed to efficiently reconstitute both myeloid and lymphoid lineages and displayed a myeloid bias ([Fig. 3 K](#) and [Fig. S1 E](#)), while their ability to contribute to the HSC compartment of the recipients was largely unaffected ([Fig. 3 L](#)). Thus, inducible *Ythdf2* deletion in adult mice causes a progressive loss of lymphoid output, myeloid bias upon aging, and an eventual failure of aged HSCs to reconstitute long-term multilineage hematopoiesis.

YTHDF2 protein expression in HSCs is induced by acute and chronic inflammation

Given that YTHDF2 expression is induced by stress in other contexts ([Yu et al., 2019](#); [Zhou et al., 2015](#)) and is known to be up-regulated in immune cells during the IFN response ([Rubio et al., 2018](#); [Winkler et al., 2019](#)), we hypothesized that YTHDF2 may itself be regulated by inflammatory stimuli in HSCs. To address this, we used *Ythdf2*^CTL mice harboring the GFP-YTHDF2
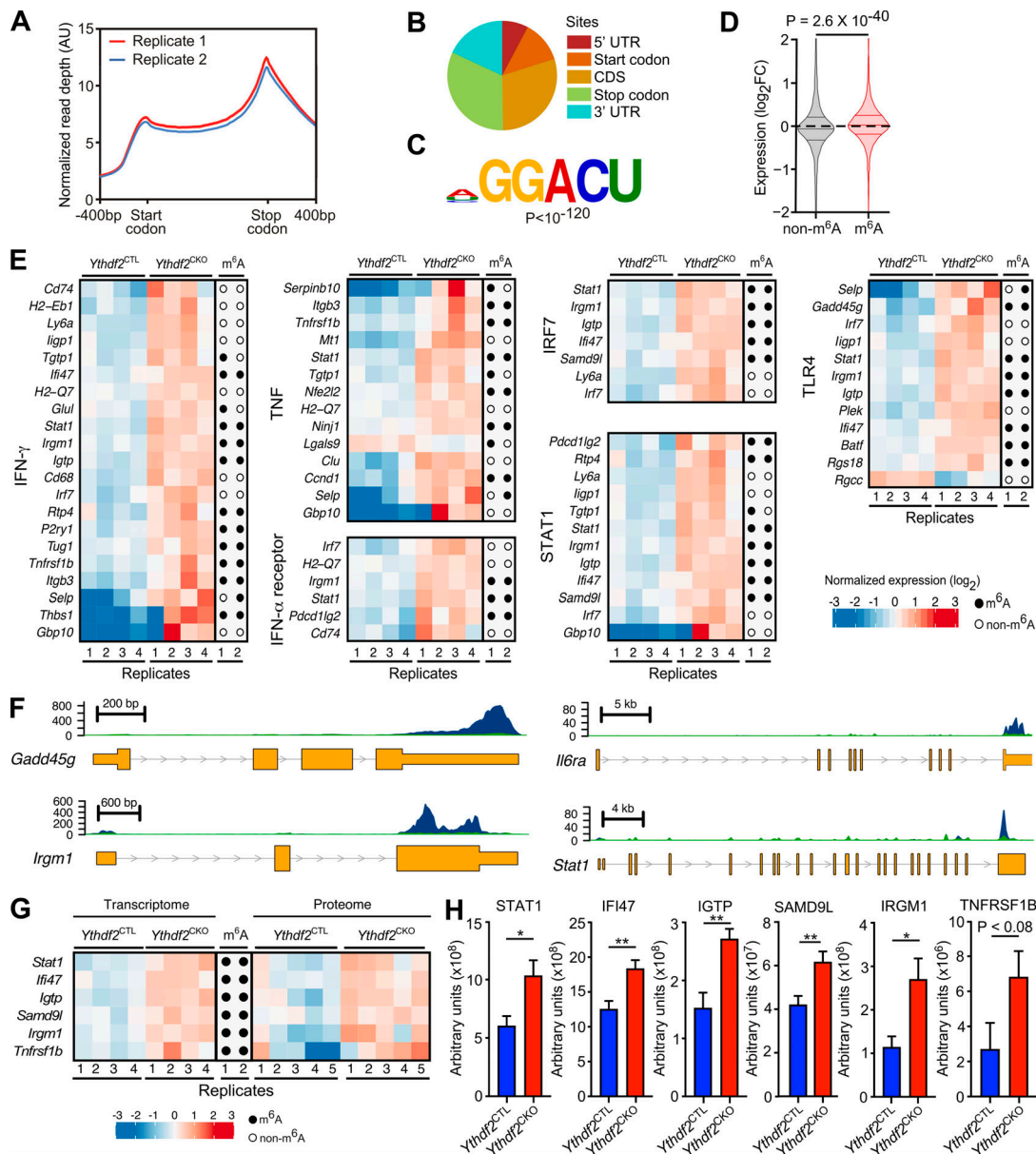
Figure 2. *Ythdf2*-deficient HSCs display up-regulation of m⁶A-modified transcripts involved in multiple proinflammatory pathways. (A) m⁶A-seq read depth along a transcript body model for two replicate c-Kit⁺ *Ythdf2*^CTL cell samples. Transcripts models were extended 400 nucleotides upstream and downstream of the start and stop codons, respectively. **(B)** Location distribution of m⁶A peaks in gene regions. m⁶A peak overlaps with different transcript regions (5′ UTR; start codon; coding sequence, CDS; stop codon; 3′ UTR). **(C)** Enriched m⁶A motif found by Homer in peaks detected by macs2 v2.1.1.20160309. **(D)** Violin plot of expression change between *Ythdf2*^CTL and *Ythdf2*^CKO BM LSK CD48⁻CD150⁺ HSCs (n = 4) from 8–12-wk-old mice for nonmethylated (nonm⁶A) and methylated (m⁶A) transcripts determined by m⁶A-seq in c-Kit⁺ cells. **(E)** Heatmaps of genes representing IPA-defined IFN-γ, TNF-α, IFN-α, IFN regulatory factor 7, STAT1 and TLR4 signaling pathways in *Ythdf2*^CKO compared with *Ythdf2*^CTL HSCs from 8–12-wk-old mice (n = 4). Transcript methylation peak presence in two replicates from c-Kit⁺ cells depicted to the right by filled (m⁶A-modified) or unfilled (no m⁶A modification detected) circles. **(F)** m⁶A signal in key transcripts involved in inflammatory responses. Read depth from two replicates of m⁶A immunoprecipitation (blue) and RNA-seq input (green). Transcript regions are depicted as exonic (yellow) and intronic (gray). **(G and H)** Methylated proinflammatory transcripts up-regulated in *Ythdf2*^CKO HSCs, which also show increased protein abundance in immortalized *Ythdf2*^CKO c-Kit⁺ cells (Paris et al., 2019). **(G)** Heatmap to left represents transcript abundance in HSC samples. Transcript m⁶A modification in c-Kit⁺ cells is indicated in the center. Heatmap to right represents protein abundance in c-Kit⁺ cells. Heatmap colors represent expression z-scores for a given row. **(H)** Peptide spectral counts (expressed as arbitrary units) from immortalized *Ythdf2*^CTL and *Ythdf2*^CKO c-Kit⁺ cells. Data represent mean ± SEM; n = 5 per genotype; *, P < 0.05; **, P < 0.01 (Mann–Whitney U test). AU, arbitrary units.

fusion protein, in which GFP analyzed by flow cytometry reports the expression of YTHDF2 protein. These mice were treated with two or eight doses of pIpC to induce the IFN-α response and model acute or chronic inflammation, respectively (Fig. 4 A). We found a significant increase in the expression of GFP-YTHDF2

protein in HSCs under both conditions (Fig. 4, B–E). Given these findings indicating that YTHDF2 is induced by inflammatory stimuli, we next examined how loss of YTHDF2 impacts the behavior of HSCs upon inflammation, by subjecting *Ythdf2*^CTL and *Ythdf2*^CKO mice to pIpC-induced chronic inflammation
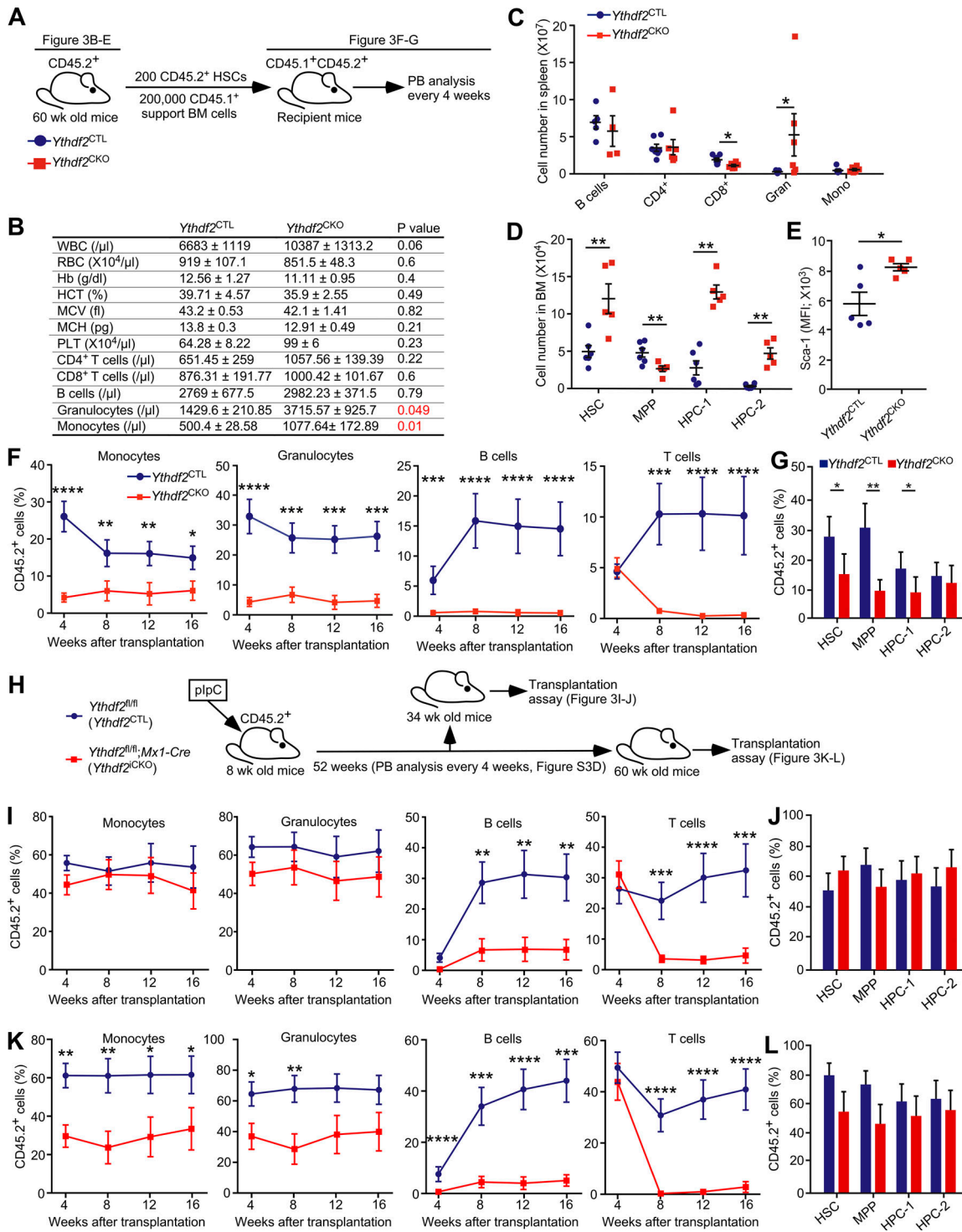
Figure 3. **HSCs lacking *Ythdf2* display a progressive myeloid bias and loss of stem cell activity upon aging. (A)** *Ythdf2*fl/fl;*Vav-iCre* (*Ythdf2*CKO) and control *Ythdf2*fl/fl (*Ythdf2*CTL) mice were aged for 1 yr, followed by analyses of their steady-state hematopoiesis (B–E). Furthermore, 200 BM LSK CD48−CD150+CD45.2+ HSCs were sorted and transplanted into lethally irradiated 8–10-wk-old syngeneic CD45.1+/CD45.2+ recipient mice (*n* = 12 per genotype) together with 2 × 10⁵ CD45.1+ competitor BM cells (F and G). **(B)** PB counts of 60–65-wk-old *Ythdf2*CKO and *Ythdf2*CTL mice (*n* ≥ 5); P < 0.05 is highlighted in red. Data represent mean ± SEM; at least two independent experiments were performed. **(C)** Total number of CD19+B220+ B cells, CD4+ T cells, CD8+ T cells, CD11b+Gr-1+ granulocytes, and CD11b+Gr-1− monocytes in spleens of 60–65-wk old *Ythdf2*CKO and *Ythdf2*CTL mice (*n* ≥ 5). Data represent mean ± SEM; *, P < 0.05 (Mann–Whitney *U* test); at least two independent experiments were performed. **(D)** Total number of HSCs, LSK CD48−CD150− MPPs, and primitive hematopoietic progenitor cells (i.e., LSK CD48+CD150− HPC-1 and LSK CD48+CD150+ HPC-2 populations) in BM of 60–65-wk-old *Ythdf2*CKO and *Ythdf2*CTL mice (*n* ≥ 5). Data represent mean ± SEM; **, P < 0.01 (Mann–Whitney *U* test); at least two independent experiments were performed. **(E)** Median Sca-1 fluorescence intensity in HSCs from 60–65-wk-old *Ythdf2*CKO or *Ythdf2*CTL mouse BM determined by flow cytometry (*n* ≥ 5). Data represent mean ± SEM; *, P < 0.05 (Mann–Whitney *U* test); at least two independent experiments were performed. **(F)** Percentage of CD45.2+ cells in the monocyte, granulocyte, B cell, and T cell compartments of

recipients transplanted with HSCs from 60–65-wk-old CD45.2$^+$ Ythdf2^{CKO} or Ythdf2^{CTL} mice (n = 12). Data represent mean ± SEM; ***, P < 0.001; ****, P < 0.0001 (Mann–Whitney U test); at least two independent experiments were performed. **(G)** Percentage of CD45.2$^+$ cells in the BM HSC, MPP, HPC-1, and HPC-2 cell compartments of recipient mice 16 wk after transplantation (n = 12). Data represent mean ± SEM; *, P < 0.05; **, P < 0.01 (Mann–Whitney U test); at least two independent experiments were performed. **(H)** 8-wk-old Ythdf2$^{fl/fl}$;Mx1-Cre (Ythdf2^{iCKO}) and control Ythdf2$^{fl/fl}$ (Ythdf2^{CTL}) mice were treated with six sequential doses of plpC (given every alternate day) to induce deletion of Ythdf2. PB samples were taken at day 0 and over a 52-wk period after pIpC treatment (Fig. S3 D). 200 BM LSK CD48$^-$CD150$^+$ CD45.2$^+$ HSCs sorted from 34-wk-old (Fig. 3, I and J) and 60-wk-old (Fig. 3, K and L) Ythdf2^{CTL} and Ythdf2^{iCKO} mice were transplanted into lethally irradiated syngeneic CD45.1$^+$/CD45.2$^+$ recipient mice together with 2 × 10^5 competitor CD45.1$^+$ BM cells (n = 12). **(I)** Percentage of CD45.2$^+$ cells overall in the monocyte, granulocyte, B cell, and T cell compartments of lethally irradiated recipient mice transplanted with HSCs from 34-wk-old CD45.2$^+$ Ythdf2^{iCKO} or Ythdf2^{CTL} mice (n = 12). Data represent mean ± SEM; **, P < 0.01; ***, P < 0.001; ****, P < 0.0001 (Mann–Whitney U test); at least two independent experiments were performed. **(J)** Percentage of CD45.2$^+$ cells in the BM HSC, MPP, HPC-1, and HPC-2 cell compartments of recipient mice 16 wk after transplantation with HSCs from 34-wk-old Ythdf2^{iCKO} or Ythdf2^{CTL} mice (n = 12). Data represent mean ± SEM, at least two independent experiments were performed. **(K)** Percentage of CD45.2$^+$ cells overall in the monocyte, granulocyte, B cell, and T cell compartments of lethally irradiated recipient mice transplanted with HSCs from 60-wk-old CD45.2$^+$ Ythdf2^{iCKO} or Ythdf2^{CTL} mice (n = 12). Data represent mean ± SEM; *, P < 0.05; **, P < 0.01; ***, P < 0.001; ****, P < 0.0001 (Mann–Whitney U test); at least two independent experiments were performed. **(L)** Percentage of CD45.2$^+$ cells in the BM HSC, MPP, HPC-1, and HPC-2 cell compartments of recipient mice 16 wk after transplantation with HSCs from 60-wk-old Ythdf2^{iCKO} or Ythdf2^{CTL} mice (n = 12). Data represent mean ± SEM; at least two independent experiments were performed.

before allowing recovery (Fig. 4 F). As in mice under steady-state conditions (Paris et al., 2019; Fig. 1 I), primitive progenitor cell populations (MPP2–4) were expanded in pIpC-treated Ythdf2^{CKO} mice compared with their Ythdf2^{CTL} counterparts (Fig. 4 G). Strikingly, however, unlike during steady-state

conditions in which Ythdf2-deficient HSCs and MPP-1 cells (also referred to as short-term HSCs) were expanded (Paris et al., 2019; Fig. 1 I), pIpC-treated Ythdf2^{CKO} and Ythdf2^{CTL} mice displayed comparable numbers of HSCs and MPP-1 cells (Fig. 4 G). Therefore, while Ythdf2-deficient HSCs (which
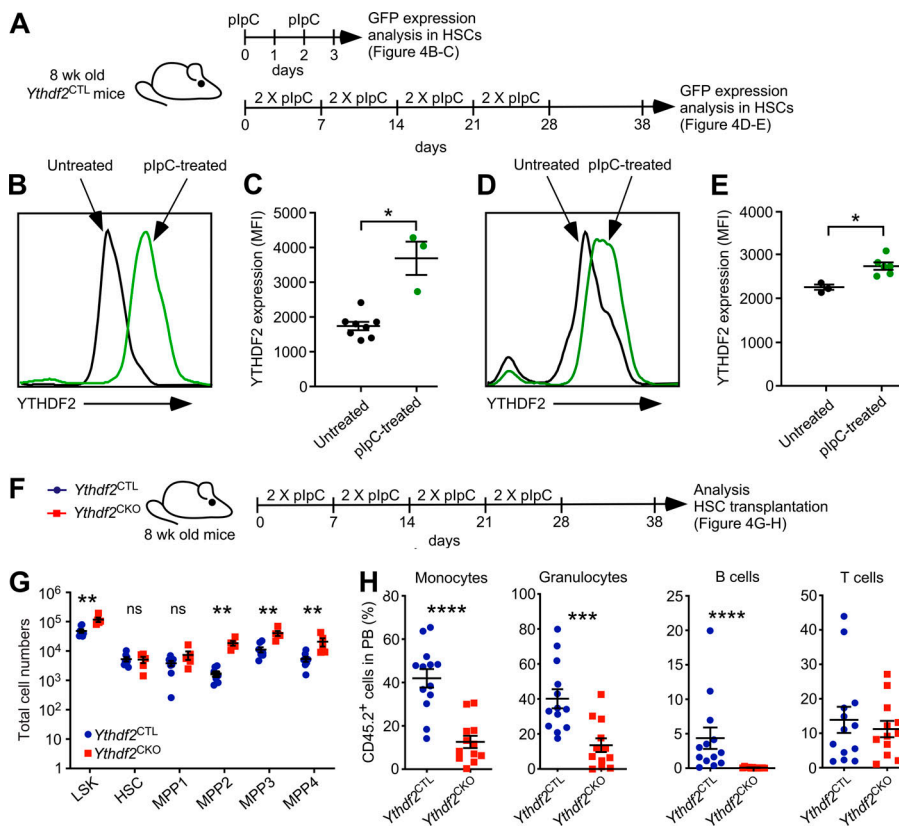
Figure 4. **YTHDF2 expression responds to acute and chronic inflammation. (A)** Ythdf2$^{fl/fl}$ (Ythdf2^{CTL}) mice were treated with two doses of plpC on days 0 and 2 before analysis on day 3 (Fig. 4, B and C) or treated with two doses of plpC per week for 4 wk and allowed to recover for 10 d before analysis (Fig. 4, D and E). Untreated littermate controls were analyzed at equal time points. **(B)** Representative histogram of modal YTHDF2-GFP fluorescence assayed by flow cytometry in LSK CD48$^-$CD150$^+$ HSCs from untreated littermate controls or mice treated with two doses of plpC. At least two independent experiments were performed. **(C)** Median YTHDF2-GFP fluorescence intensity (MFI) of the data presented in B (n = 3 and n = 8 biological replicates, for treated and untreated, respectively). Data represent mean ± SEM; *, P < 0.05; (Mann–Whitney U test); at least two independent experiments were performed. **(D)** Representative histogram of modal YTHDF2-GFP fluorescence assayed by flow cytometry in HSCs from untreated littermate controls or mice treated with two doses of plpC weekly for 4 wk followed by 10-d recovery before analysis. At least two independent experiments were performed. **(E)** YTHDF2-GFP MFI of the data shown in D (n = 5 and n = 3 biological replicates, for treated and untreated, respectively). Data represent mean ± SEM; *, P < 0.05 (Mann–Whitney U test); at least two independent experiments were performed. **(F)** Ythdf2$^{fl/fl}$;Vav-iCre (Ythdf2^{CKO}) and control Ythdf2$^{fl/fl}$ (Ythdf2^{CTL}) mice were treated with two doses of plpC per week for 4 wk and allowed to recover for 10 d before analysis (Fig. 4 G). Furthermore, 200 LSK CD48$^-$CD150$^+$ CD45.2$^+$ BM HSCs were sorted and transplanted into lethally irradiated 8–10-wk-old syngeneic CD45.1$^+$/CD45.2$^+$ recipient mice (n = 12 per genotype) together with 2 × 10^5 CD45.1$^+$ competitor BM cells (Fig. 4 H). **(G)** Total number of lineage$^-$Sca-1$^+$c-Kit$^+$ LSK cells, HSCs (LSK CD34$^-$CD135$^-$CD150$^+$CD48$^-$), MPP1 (LSK CD34$^+$CD135$^-$CD150$^+$CD48$^-$), MPP2 (LSK CD34$^+$CD135$^-$CD150$^+$CD48$^+$), MPP3 (LSK CD34$^+$CD135$^-$CD150$^-$CD48$^+$), and MPP4 (LSK CD34$^+$CD135$^+$CD150$^-$CD48$^+$) cell populations in the BM of plpC-treated Ythdf2^{CKO} or Ythdf2^{CTL} mice. Data represent mean ± SEM; **, P < 0.01; ns, not significant (Mann–Whitney U test); at least two independent experiments were performed. **(H)** Percentage of CD45.2$^+$ cells in the CD11b$^+$Gr-1$^-$ monocyte, CD11b$^+$Gr-1$^+$ granulocyte, CD19$^+$ B cell, and CD4$^+$ or CD8$^+$ T cell, compartments of recipients transplanted with HSCs from plpC treatedYthdf2^{CKO} or Ythdf2^{CTL} mice 1 mo after transplantation (n = 12 and n = 13 recipients, respectively). Data represent mean ± SEM; ***, P < 0.001; ****, P < 0.0001 (Mann–Whitney U test); at least two independent experiments were performed.

display up-regulated proinflammatory pathways) undergo expansion under steady-state conditions, additional inflammatory stimuli abrogate this phenotype.

Finally, to investigate whether *Ythdf2* deficiency in HSCs had any impact on their short-term reconstitution potential upon pIpC administration, we competitively transplanted equal numbers of HSCs from pIpC-treated *Ythdf2*CKO and *Ythdf2*CTL mice into lethally irradiated recipients (Fig. 4 F). HSCs lacking *Ythdf2* displayed decreased short-term myeloid and B-lymphoid reconstitution capacity, indicating that inflammation temporarily weakened *Ythdf2*-deficient HSC activity (Fig. 4 H). Thus, our data indicate that YTHDF2 is induced by inflammation in HSCs and suggest that YTHDF2 may function to protect HSCs from excessive proinflammatory signals. The mechanisms through which YTHDF2 is induced by inflammation, and its precise involvement in protecting HSCs in this context, remain important open questions meriting further investigations.

Collectively, YTHDF2 expression is induced in HSCs by inflammatory stimuli and its deletion results in constitutive activation of proinflammatory pathways, consistent with myeloid bias. While YTHDF2 is not essential for long-term steady-state unperturbed hematopoiesis upon aging, *Ythdf2* deletion causes progressive HSC expansion and failure of HSCs to reconstitute multilineage hematopoiesis. Because the activation of inflammatory pathways in HSCs by infections or injury causes their proliferation and myeloid cell production, but in the longer term compromises HSC activity (Esplin et al., 2011; Essers et al., 2009; Pietras, 2017; Takizawa et al., 2017), HSCs must use mechanisms to counteract these signals and protect their long-term integrity. While several studies indicated that proinflammatory signals are suppressed in HSCs at different levels of gene expression, including cell signaling, gene transcription, and RNA editing (Hartner et al., 2009; King et al., 2011; Sato et al., 2009), the functional significance of dynamic RNA modifications in this important aspect of HSC biology remains poorly understood. We suggest that the m6A-dependent mRNA decay pathway is a novel mechanism through which HSCs suppress inflammation and sustain HSC integrity. Interrogation of up-regulated proinflammatory genes upon *Ythdf2* deficiency in genetic rescue approaches is warranted to further support this notion. Given our findings that YTHDF2 itself is induced by inflammation, we suggest that YTHDF2 may function in a negative feedback loop to prevent an excessive inflammatory response detrimental to HSC function. Thus, our work sets the stage for further investigations focusing on how YTHDF2 regulates HSC fates during inflammation upon acute and chronic infection. In closing, our data position YTHDF2 as an essential repressor of proinflammatory pathways in HSCs and highlight the key significance of m6A mRNA modification in long-term HSC maintenance upon aging.

Materials and methods

Mice
All mice were on the C57BL/6 background (backcrossed for ≥10 generations). *Ythdf2*fl/fl, *Vav-iCre*, and *Mx1-Cre* strains have been described previously (de Boer et al., 2003; Ivanova et al., 2017; Kühn et al., 1995). Congenic recipient mice were CD45.1+/CD45.2+.

All experiments involving mice were performed under University of Edinburgh Veterinary oversight with UK Home Office authorization. All control mice were littermates, and treatment groups were randomized among littermates.

Flow cytometry
BM and splenic cells were prepared and analyzed as described previously (Guitart et al., 2017; Guitart et al., 2013; Kranc et al., 2009; Mortensen et al., 2011; Paris et al., 2019; Vukovic et al., 2016). Hematopoietic stem and progenitor cell staining began with incubation with Fc block followed by biotin-conjugated anti-Lineage marker antibodies (anti-CD4, anti-CD5, anti-CD8a, anti-CD11b, anti-B220, anti-Gr-1, and anti-Ter119), APC-conjugated anti-c-Kit, APC-Cy7–conjugated anti-Sca-1, PE-conjugated anti-CD48, and PE-Cy7–conjugated anti-CD150 antibodies. Biotin-conjugated lineage markers were then stained with PerCP-conjugated streptavidin. Staining of MPP1–4 populations was performed as above for hematopoietic stem and progenitor cells; however, BV711- instead of APC-conjugated anti-c-Kit was used and cells were also stained with APC-conjugated anti-Flt3– and BV421-conjugated anti-CD34 antibodies.

For PB and differentiated cell analysis, cells were stained with PerCP-conjugated anti-B220, APC-Cy7–conjugated anti-CD19, Pacific Blue–conjugated anti-CD11b, PE-Cy7–conjugated anti-Gr-1, APC-conjugated anti-CD8, and PE-conjugated anti-CD4 antibodies. To distinguish CD45.2 chimerism in transplantation experiments, BV711-conjugated anti-CD45.1 and Pacific Blue–conjugated anti-CD45.2 antibodies were used. For hematopoietic stem and progenitor cell staining in transplanted mice, APC-conjugated anti-c-Kit and APC-Cy7-conjugated anti-Sca-1 were used; the remainder of the staining was as described above. For analyses of differentiated cells and PB in transplanted mice, cell suspensions were stained with BV711-conjugated anti-CD45.1, Pacific Blue–conjugated anti-CD45.2, APC-conjugated anti-CD11b, PE-Cy7–conjugated anti-Gr-1, PE-conjugated anti-CD4 and -CD8a, and APC-Cy7–conjugated anti-CD19. Flow cytometry analyses were performed using a LSRFortessa (BD Biosciences). Cell sorting was performed on a FACSAria Fusion (BD Biosciences).

Intracellular staining and flow cytometry analysis
BM and splenic cells were prepared and analyzed as described previously (Guitart et al., 2017; Guitart et al., 2013; Kranc et al., 2009; Mortensen et al., 2011; Paris et al., 2019; Vukovic et al., 2016) followed by c-Kit enrichment (described below). Cells were incubated with Fc block and stained with biotin-conjugated anti-Lineage marker antibodies (anti-CD4, anti-CD5, anti-CD8a, anti-CD11b, anti-B220, anti-Gr-1, and anti-Ter119), APC-Cy7–conjugated anti-c-Kit, and Pacific Blue–conjugated anti-Sca-1. Biotin-conjugated Lineage markers were then stained with PerCP-conjugated Streptavidin. Cells were then fixed and permeabilized using Phosflow Lyse/Fix, Phosflow Perm Buffer III, and stain buffer (all from BD Biosciences) according to the manufacturer's instructions. After processing, cells were stained with AF647-conjugated anti-pStat1 or anti-pStat3.

Syngeneic transplantation assays
Transplant recipient CD45.1+/CD45.2+ mice were lethally irradiated with two doses of 5.5 Gy administered ≥4 h apart at an

Mapperley et al.
YTHDF2 suppresses inflammation to sustain HSCs

Journal of Experimental Medicine   8 of 11
https://doi.org/10.1084/jem.20200829

average rate of 0.58 Gy/min using a cesium-137 GammaCell 40 irradiator. For primary transplantations, irradiated recipient CD45.1$^+$/CD45.2$^+$ mice were intravenously injected with 200 LSK CD48$^-$CD150$^+$ HSCs and 200,000 support CD45.1$^+$ unfractionated BM cells. For secondary transplantations, recipient CD45.1$^+$/CD45.2$^+$ mice were intravenously injected with 2,000 CD45.2$^+$ LSK cells or 100,000 c-Kit–enriched BM cells from primary recipients and 200,000 support CD45.1$^+$ unfractionated BM cells. All recipient mice were culled and analyzed 16–20 wk after transplantation. A minimum of two independent donor mice were used for all transplantations.

pIpC administration

For gene deletion via activation of the *Mx1-Cre* promotor, mice were injected i.p. every other day with 300 µg pIpC (GE Healthcare) for a total of six doses over 11 d, as previously described (Guitart et al., 2017; Guitart et al., 2013; Kranc et al., 2009; Paris et al., 2019), and gene deletion was assayed by YTHDF2-GFP fusion protein fluorescence. To test the effect of innate immune activation, mice were injected i.p. with 300 µg pIpC (GE Healthcare) as described per experiment.

CD117 (c-Kit) enrichment

Enrichment for cells expressing CD117 (c-Kit) was performed using CD117 MicroBeads and LS columns from Miltenyi Biotec, according to the manufacturer's instructions.

Histology

Tibias and femurs were dissected and cleaned before fixation in 4% paraformaldehyde for 24 h. Fixed bones were decalcified, embedded in paraffin, and sectioned. Sections were stained with H&E and mounted. Whole sections were imaged using a Vectra Polaris slide scanner, and representative images were taken at 10× and 20× magnification.

RNA-seq

100 HSCs per sample were sorted into 0.4% Triton X-100, RNase inhibitor, 10 mM dNTPs, and 10 µM Oligo dT before RNA-seq by SMART-Seq2 in the Single Cell Genomics Facility at the Medical Research Council Weatherall Institute of Molecular Medicine (University of Oxford). Alignments to the GRCm38 mouse genome were performed using HISAT2 (Kim et al., 2015), and further analysis was performed in R. Counts were assigned to genes using the Rsubread package, and quality control analysis of the samples was performed with the SingleCellExperiment and scater packages. Differentially expressed genes were identified using likelihood ratio tests computed by the edgeR package. The RNA-seq dataset was deposited in GEO (accession no. GSE142019).

m^{6}A meRIP-seq

m^{6}A meRIP-seq library preparation was performed as previously described (Lin et al., 2016) from *Ythdf2*^{CTL} c-Kit–enriched cells. Reads from two biological replicates were aligned to the mouse GRCm38 genome using HISAT2 (Kim et al., 2015), and peaks were called using MACS2, version 2.1.1 with the nomodel flag (Zhang et al., 2008). To analyze the distribution of

m^{6}A-associated reads along the transcripts, treat_pileup bedgraph file outputs from MACS2 were converted to bigWig format and used as input for the computeMatrix function of the deepTools package, version 2.5.5 (Ramírez et al., 2014). Motif enrichment was done using Homer, version 4.10, selecting a motif length of six nucleotides. Background regions were generated by shuffling peaks along the transcriptome using the shuffleBed tool from the bedtools suite, version 2.28 (Quinlan and Hall, 2010). The GVIZ bioconductor package was used for peak visualization (Hahne and Ivanek, 2016). m^{6}A meRIP-seq dataset was deposited in GEO (accession no. GSE142020).

GSEA and IPA

GSEA was performed using GSEA software version 3.0 with 1,000 permutations and default parameters. Gene differential expression, computed by the edgeR package in R, was ranked by moderated *t* statistics, which takes into account variability between genes in the ranking. Ranked genes were compared with gene lists in the Hallmark subset of the MSigDB database, version 7.0. IPA was performed using the Core Analysis Function offered by Qiagen's Ingenuity Pathway Analysis software (Krämer et al., 2014). The interrogated RNA-seq and mass spectrometry datasets were filtered for adjusted P values of differential expression (FDR < 0.05), and the threshold for significant activation or inhibition was defined by an absolute Z-score value >2.

SLAM-seq analysis

The SLAM-seq dataset (Paris et al., 2019) was analyzed using the SlamDunk pipeline (Herzog et al., 2017).

Mass spectroscopy analysis

Immortalized *Ythdf2*^{CKO} and *Ythdf2*^{CTL} c-Kit–enriched cells (Paris et al., 2019) were pelleted, lysed, and processed according to (Wiśniewski and Rakus, 2014). Tryptic peptides were analyzed on a QExactive+ mass spectrometer connected to an Ultimate Ultra3000 chromatography system packed with 1.8 µm uChrom and separated by an acetonitrile gradient. Mass spectra were analyzed using MaxQuant against the Uniprot mouse database proteome, ID UP000000589.

Quantification and statistical analysis

Statistical analyses were performed using Prism 6 software (GraphPad Software). P values were calculated using a two-tailed Mann–Whitney *U* test unless stated otherwise.

Online supplemental material

Fig. S1 shows the frequency of B cells, T cells, granulocytes, and monocytes within the CD45.2$^+$ donor-derived population of PB, BM, and spleen from transplant recipients shown in Figs. 1 B; and 3 F, I, and K. Also shown are GSEA plots from RNA-seq of *Ythdf2*^{CKO} and *Ythdf2*^{CTL} HSCs from Fig. 1 F. Fig. S2 shows IPA of RNA-seq and mass spectrometry from *Ythdf2*^{CKO} and *Ythdf2*^{CTL} cells and mRNA decay curves for transcripts of interest within *Ythdf2*^{CKO} and *Ythdf2*^{CTL} c-Kit$^+$ cells. Fig. S3 shows data to support our conclusions in aged mice (YTHDF2-GFP mean fluorescence is not significantly altered with age; aged mice have

normal BM cellularity and histology); percentage of monocytes, granulocytes, CD4^{+} T cells, CD8^{+} T cells, B cells, and GFP^{+} cells in PB from mice 1 yr after *Ythdf2* deletion; and total blood counts, numbers of differentiated cells, and numbers of HSCs for mice 1 yr after *Ythdf2* deletion.

Acknowledgments

References

Barbieri, I., K. Tzelepis, L. Pandolfini, J. Shi, G. Millán-Zambrano, S.C. Robson, D. Aspris, V. Migliori, A.J. Bannister, N. Han, et al. 2017. Promoter-bound METTL3 maintains myeloid leukaemia by m6A-dependent translation control. *Nature.* 552:126–131. https://doi.org/10.1038/nature24678

Cheng, Y., H. Luo, F. Izzo, B.F. Pickering, D. Nguyen, R. Myers, A. Schurer, S. Gourkanti, J.C. Brüning, L.P. Vu, et al. 2019. m6A RNA Methylation Maintains Hematopoietic Stem Cell Identity and Symmetric Commitment. *Cell Rep.* 28:1703–1716.e6.

de Boer, J., A. Williams, G. Skavdis, N. Harker, M. Coles, M. Tolaini, T. Norton, K. Williams, K. Roderick, A.J. Potocnik, and D. Kioussis. 2003. Transgenic mice with hematopoietic and lymphoid specific expression of Cre. *Eur. J. Immunol.* 33:314–325. https://doi.org/10.1002/immu.200310005

Du, H., Y. Zhao, J. He, Y. Zhang, H. Xi, M. Liu, J. Ma, and L. Wu. 2016. YTHDF2 destabilizes m(6)A-containing RNA through direct recruitment of the CCR4-NOT deadenylase complex. *Nat. Commun.* 7:12626. https://doi.org/10.1038/ncomms12626

Esplin, B.L., T. Shimazu, R.S. Welner, K.P. Garrett, L. Nie, Q. Zhang, M.B. Humphrey, Q. Yang, L.A. Borghesi, and P.W. Kincade. 2011. Chronic exposure to a TLR ligand injures hematopoietic stem cells. *J. Immunol.* 186:5367–5375. https://doi.org/10.4049/jimmunol.1003438

Essers, M.A., S. Offner, W.E. Blanco-Bose, Z. Waibler, U. Kalinke, M.A. Duchosal, and A. Trumpp. 2009. IFNalpha activates dormant haematopoietic stem cells in vivo. *Nature.* 458:904–908. https://doi.org/10.1038/nature07815

Frye, M., B.T. Harada, M. Behm, and C. He. 2018. RNA modifications modulate gene expression during development. *Science.* 361:1346–1349. https://doi.org/10.1126/science.aau1646

Guitart, A.V., T.I. Panagopoulou, A. Villacreces, M. Vukovic, C. Sepulveda, L. Allen, R.N. Carter, L.N. van de Lagemaat, M. Morgan, P. Giles, et al. 2017. Fumarate hydratase is a critical metabolic regulator of hematopoietic stem cell functions. *J. Exp. Med.* 214:719–735. https://doi.org/10.1084/jem.20161087

Guitart, A.V., C. Subramani, A. Armesilla-Diaz, G. Smith, C. Sepulveda, D. Gezer, M. Vukovic, K. Dunn, P. Pollard, T.L. Holyoake, et al. 2013. Hif-2α is not essential for cell-autonomous hematopoietic stem cell maintenance. *Blood.* 122:1741–1745. https://doi.org/10.1182/blood-2013-02-484923

Hahne, F., and R. Ivanek. 2016. Visualizing Genomic Data Using Gviz and Bioconductor. *Methods Mol. Biol.* 1418:335–351. https://doi.org/10.1007/978-1-4939-3578-9_16

Hartner, J.C., C.R. Walkley, J. Lu, and S.H. Orkin. 2009. ADAR1 is essential for the maintenance of hematopoiesis and suppression of interferon signaling. *Nat. Immunol.* 10:109–115. https://doi.org/10.1038/ni.1680

Herzog, V.A., B. Reichholf, T. Neumann, P. Rescheneder, P. Bhat, T.R. Burkard, W. Wlotzka, A. von Haeseler, J. Zuber, and S.L. Ameres. 2017. Thiol-linked alkylation of RNA to assess expression dynamics. *Nat. Methods.* 14:1198–1204. https://doi.org/10.1038/nmeth.4435

Ivanova, I., C. Much, M. Di Giacomo, C. Azzi, M. Morgan, P.N. Moreira, J. Monahan, C. Carrieri, A.J. Enright, and D. O'Carroll. 2017. The RNA m6A Reader YTHDF2 Is Essential for the Post-transcriptional Regulation of the Maternal Transcriptome and Oocyte Competence. *Mol. Cell.* 67:1059–1067.e4.

Kim, D., B. Langmead, and S.L. Salzberg. 2015. HISAT: a fast spliced aligner with low memory requirements. *Nat. Methods.* 12:357–360. https://doi.org/10.1038/nmeth.3317

King, K.Y., M.T. Baldridge, D.C. Weksberg, S.M. Chambers, G.L. Lukov, S. Wu, N.C. Boles, S.Y. Jung, J. Qin, D. Liu, et al. 2011. Irgm1 protects hematopoietic stem cells by negative regulation of IFN signaling. *Blood.* 118:1525–1533. https://doi.org/10.1182/blood-2011-01-328682

Krämer, A., J. Green, J. Pollard Jr., and S. Tugendreich. 2014. Causal analysis approaches in Ingenuity Pathway Analysis. *Bioinformatics.* 30:523–530. https://doi.org/10.1093/bioinformatics/btt703

Kranc, K.R., H. Schepers, N.P. Rodrigues, S. Bamforth, E. Villadsen, H. Ferry, T. Bouriez-Jones, M. Sigvardsson, S. Bhattacharya, S.E. Jacobsen, and T. Enver. 2009. Cited2 is an essential regulator of adult hematopoietic stem cells. *Cell Stem Cell.* 5:659–665. https://doi.org/10.1016/j.stem.2009.11.001

Kühn, R., F. Schwenk, M. Aguet, and K. Rajewsky. 1995. Inducible gene targeting in mice. *Science.* 269:1427–1429. https://doi.org/10.1126/science.7660125

Li, Z., P. Qian, W. Shao, H. Shi, X.C. He, M. Gogol, Z. Yu, Y. Wang, M. Qi, Y. Zhu, et al. 2018. Suppression of m6A reader Ythdf2 promotes hematopoietic stem cell expansion. *Cell Res.* 28:904–917. https://doi.org/10.1038/s41422-018-0072-0

Li, Z., H. Weng, R. Su, X. Weng, Z. Zuo, C. Li, H. Huang, S. Nachtergaele, L. Dong, C. Hu, et al. 2017. FTO Plays an Oncogenic Role in Acute Myeloid Leukemia as a N6-Methyladenosine RNA Demethylase. *Cancer Cell.* 31: 127–141. https://doi.org/10.1016/j.ccell.2016.11.017

Lin, S., J. Choe, P. Du, R. Triboulet, and R.I. Gregory. 2016. The m(6)A Methyltransferase METTL3 Promotes Translation in Human Cancer Cells. *Mol. Cell.* 62:335–345. https://doi.org/10.1016/j.molcel.2016.03.021

Mortensen, M., E.J. Soilleux, G. Djordjevic, R. Tripp, M. Lutteropp, E. Sadighi-Akha, A.J. Stranks, J. Glanville, S. Knight, S.-E.W. Jacobsen, et al. 2011.

The autophagy protein Atg7 is essential for hematopoietic stem cell maintenance. *J. Exp. Med.* 208:455–467. https://doi.org/10.1084/jem .20101145

Paris, J., M. Morgan, J. Campos, G.J. Spencer, A. Shmakova, I. Ivanova, C. Mapperley, H. Lawson, D.A. Wotherspoon, C. Sepulveda, et al. 2019. Targeting the RNA m⁶A Reader YTHDF2 Selectively Compromises Cancer Stem Cells in Acute Myeloid Leukemia. *Cell Stem Cell.* 25: 137–148.e6. https://doi.org/10.1016/j.stem.2019.03.021

Pietras, E.M. 2017. Inflammation: a key regulator of hematopoietic stem cell fate in health and disease. *Blood.* 130:1693–1698. https://doi.org/10.1182/ blood-2017-06-780882

Pietras, E.M., R. Lakshminarasimhan, J.M. Techner, S. Fong, J. Flach, M. Binnewies, and E. Passegué. 2014. Re-entry into quiescence protects hematopoietic stem cells from the killing effect of chronic exposure to type I interferons. *J. Exp. Med.* 211:245–262. https://doi.org/10.1084/jem.20131043

Pietras, E.M., C. Mirantes-Barbeito, S. Fong, D. Loeffler, L.V. Kovtonyuk, S. Zhang, R. Lakshminarasimhan, C.P. Chin, J.M. Techner, B. Will, et al. 2016. Chronic interleukin-1 exposure drives haematopoietic stem cells towards precocious myeloid differentiation at the expense of self-renewal. *Nat. Cell Biol.* 18:607–618. https://doi.org/10.1038/ncb3346

Pietras, E.M., D. Reynaud, Y.A. Kang, D. Carlin, F.J. Calero-Nieto, A.D. Leavitt, J.M. Stuart, B. Göttgens, and E. Passegué. 2015. Functionally Distinct Subsets of Lineage-Biased Multipotent Progenitors Control Blood Production in Normal and Regenerative Conditions. *Cell Stem Cell.* 17:35–46. https://doi.org/10.1016/j.stem.2015.05.003

Quinlan, A.R., and I.M. Hall. 2010. BEDTools: a flexible suite of utilities for comparing genomic features. *Bioinformatics.* 26:841–842. https://doi .org/10.1093/bioinformatics/btq033

Ramírez, F., F. Dündar, S. Diehl, B.A. Grüning, and T. Manke. 2014. deepTools: a flexible platform for exploring deep-sequencing data. *Nucleic Acids Res.* 42(Web Server issue, W1):W187-91. https://doi.org/10.1093/nar/gku365

Rubio, R.M., D.P. Depledge, C. Bianco, L. Thompson, and I. Mohr. 2018. RNA m⁶ A modification enzymes shape innate responses to DNA by regulating interferon β. *Genes Dev.* 32:1472–1484. https://doi.org/10.1101/gad .319475.118

Sato, T., N. Onai, H. Yoshihara, F. Arai, T. Suda, and T. Ohteki. 2009. Interferon regulatory factor-2 protects quiescent hematopoietic stem cells from type I interferon-dependent exhaustion. *Nat. Med.* 15:696–700. https://doi.org/10.1038/nm.1973

Takizawa, H., K. Fritsch, L.V. Kovtonyuk, Y. Saito, C. Yakkala, K. Jacobs, A.K. Ahuja, M. Lopes, A. Hausmann, W.D. Hardt, et al. 2017. Pathogen-Induced TLR4-TRIF Innate Immune Signaling in Hematopoietic Stem Cells Promotes Proliferation but Reduces Competitive Fitness. *Cell Stem Cell.* 21:225–240.e5. https://doi.org/10.1016/j.stem.2017.06.013

Vu, L.P., Y. Cheng, and M.G. Kharas. 2019. The Biology of m⁶A RNA Methylation in Normal and Malignant Hematopoiesis. *Cancer Discov.* 9:25–33. https://doi.org/10.1158/2159-8290.CD-18-0959

Vu, L.P., B.F. Pickering, Y. Cheng, S. Zaccara, D. Nguyen, G. Minuesa, T. Chou, A. Chow, Y. Saletore, M. MacKay, et al. 2017. The N⁶-methyladenosine (m⁶A)-forming enzyme METTL3 controls myeloid differentiation of normal hematopoietic and leukemia cells. *Nat. Med.* 23:1369–1376. https://doi.org/10.1038/nm.4416

Vukovic, M., C. Sepulveda, C. Subramani, A.V. Guitart, J. Mohr, L. Allen, T.I. Panagopoulou, J. Paris, H. Lawson, A. Villacreces, et al. 2016. Adult hematopoietic stem cells lacking Hif-1α self-renew normally. *Blood.* 127: 2841–2846. https://doi.org/10.1182/blood-2015-10-677138

Wang, H., H. Zuo, J. Liu, F. Wen, Y. Gao, X. Zhu, B. Liu, F. Xiao, W. Wang, G. Huang, et al. 2018. Loss of YTHDF2-mediated m⁶A-dependent mRNA clearance facilitates hematopoietic stem cell regeneration. *Cell Res.* 28: 1035–1038. https://doi.org/10.1038/s41422-018-0082-y

Wang, X., Z. Lu, A. Gomez, G.C. Hon, Y. Yue, D. Han, Y. Fu, M. Parisien, Q. Dai, G. Jia, et al. 2014. N6-methyladenosine-dependent regulation of messenger RNA stability. *Nature.* 505:117–120. https://doi.org/10.1038/ nature12730

Wang, X., B.S. Zhao, I.A. Roundtree, Z. Lu, D. Han, H. Ma, X. Weng, K. Chen, H. Shi, and C. He. 2015. N(6)-methyladenosine Modulates Messenger RNA Translation Efficiency. *Cell.* 161:1388–1399. https://doi.org/10.1016/ j.cell.2015.05.014

Weng, H., H. Huang, H. Wu, X. Qin, B.S. Zhao, L. Dong, H. Shi, J. Skibbe, C. Shen, C. Hu, et al. 2018. METTL14 Inhibits Hematopoietic Stem/Progenitor Differentiation and Promotes Leukemogenesis via mRNA m⁶A Modification. *Cell Stem Cell.* 22:191–205.e9. https://doi.org/10.1016/j .stem.2017.11.016

Winkler, R., E. Gillis, L. Lasman, M. Safra, S. Geula, C. Soyris, A. Nachshon, J. Tai-Schmiedel, N. Friedman, V.T.K. Le-Trilling, et al. 2019. m⁶A modification controls the innate immune response to infection by targeting type I interferons. *Nat. Immunol.* 20:173–182. https://doi.org/10.1038/ s41590-018-0275-z

Wiśniewski, J.R., and D. Rakus. 2014. Multi-enzyme digestion FASP and the 'Total Protein Approach'-based absolute quantification of the Escherichia coli proteome. *J. Proteomics.* 109:322–331. https://doi.org/10.1016/j .jprot.2014.07.012

Yamashita, M., and E. Passegué. 2019. TNF-α Coordinates Hematopoietic Stem Cell Survival and Myeloid Regeneration. *Cell Stem Cell.* 25: 357–372.e7. https://doi.org/10.1016/j.stem.2019.05.019

Yu, R., Q. Li, Z. Feng, L. Cai, and Q. Xu. 2019. m6A Reader YTHDF2 Regulates LPS-Induced Inflammatory Response. *Int. J. Mol. Sci.* 20:1323. https:// doi.org/10.3390/ijms20061323

Zhang, B., D. Oyewole-Said, J. Zou, I.R. Willliams, and A.T. Gewirtz. 2017. TLR5 signaling in murine bone marrow induces hematopoietic progenitor cell proliferation and aids survival from radiation. *Blood Adv.* 1: 1796–1806. https://doi.org/10.1182/bloodadvances.2017006981

Zhang, H., S. Rodriguez, L. Wang, S. Wang, H. Serezani, R. Kapur, A.A. Cardoso, and N. Carlesso. 2016. Sepsis Induces Hematopoietic Stem Cell Exhaustion and Myelosuppression through Distinct Contributions of TRIF and MYD88. *Stem Cell Reports.* 6:940–956. https://doi.org/10.1016/j .stemcr.2016.05.002

Zhang, Y., T. Liu, C.A. Meyer, J. Eeckhoute, D.S. Johnson, B.E. Bernstein, C. Nusbaum, R.M. Myers, M. Brown, W. Li, and X.S. Liu. 2008. Model-based analysis of ChIP-Seq (MACS). *Genome Biol.* 9:R137. https://doi .org/10.1186/gb-2008-9-9-r137

Zhou, J., J. Wan, X. Gao, X. Zhang, S.R. Jaffrey, and S.B. Qian. 2015. Dynamic m(6)A mRNA methylation directs translational control of heat shock response. *Nature.* 526:591–594. https://doi.org/10.1038/nature15377

Supplemental material
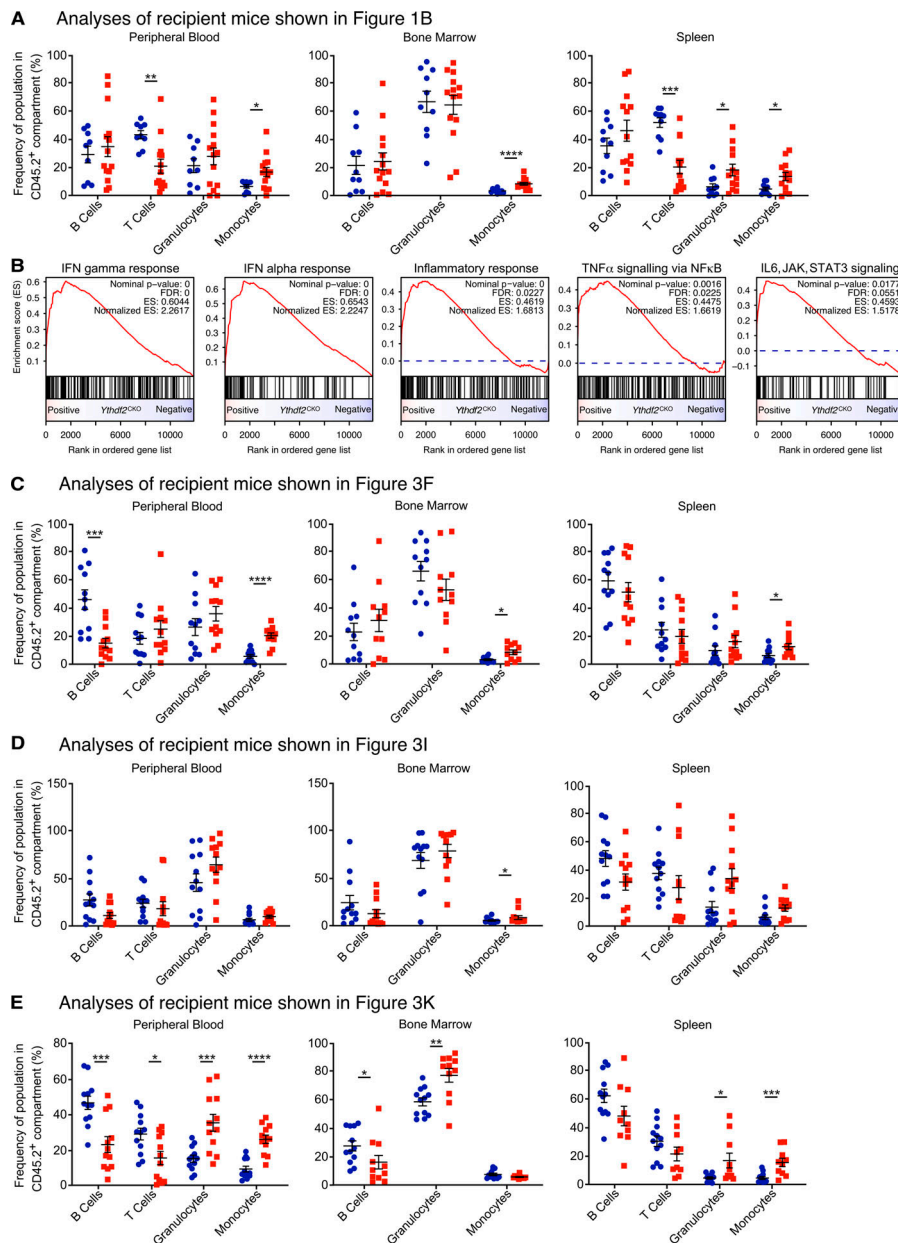
Figure S1. Molecular and cellular features of *Ythdf2*-deficient HSCs. (A) BM LSK CD48⁻CD150⁺CD45.2⁺ HSCs from 8-wk-old *Ythdf2*^CKO and *Ythdf2*^CTL mice were transplanted to lethally irradiated syngeneic CD45.1⁺/CD45.2⁺ primary recipient mice together with 2 × 10⁵ competitor CD45.1⁺ BM cells (as published in Paris et al., 2019). After 16 wk, 2,000 CD45.2⁺ LSK cells were sorted from primary recipient mice and transplanted into lethally irradiated syngeneic CD45.1⁺/CD45.2⁺ secondary recipient mice together with 2 × 10⁵ competitor CD45.1⁺ BM cells (as described in Fig. 1 A). The frequency of CD19⁺ B cells, CD4⁺ or CD8⁺ T cells, CD11b⁺Gr-1⁺ granulocytes, and CD11b⁺Gr-1⁻ monocytes in the CD45.2⁺ compartment of PB, BM, and spleen of secondary transplanted mice was analyzed 16 wk after transplantation. Analysis of the percentage of CD45.2⁺ cells in each compartment is presented in Fig. 1, B and C (*n* = 12). Data represent mean ± SEM; *, P < 0.05; **, P < 0.01; ***, P < 0.001; ****, P < 0.0001 (Mann–Whitney *U* test); at least two independent experiments were performed. **(B)** HSCs lacking *Ythdf2* display proinflammatory gene signatures. GSEA of differential gene expression in *Ythdf2*^CKO versus *Ythdf2*^CTL HSCs from young animals. Results for five significant (FDR < 0.1) inflammation-related categories are shown (Hallmark, MSigDB v6.2). Genes were ordered by log P value but ranked in the same sense as log fold-change. **(C)** *Ythdf2*^CKO and control *Ythdf2*^CTL mice were aged for 1 yr before sorting and transplantation of 200 BM LSK CD48⁻CD150⁺CD45.2⁺ HSCs into lethally irradiated 8–10-wk-old syngeneic CD45.1⁺/CD45.2⁺ recipient mice (*n* = 12) together with 2 × 10⁵ CD45.1⁺ competitor BM cells (as described in Fig. 3 A). After 16 wk, the frequency of B cells, T cells, granulocytes, and monocytes in the CD45.2⁺ compartment of PB, BM, and spleen of recipient mice was analyzed. Analysis of the percentage of CD45.2⁺ cells within lineages and stem cell compartments is presented in Fig. 3, F and G. Data represent mean ± SEM; *, P < 0.05; ***, P < 0.001; ****, P < 0.0001 (Mann–Whitney *U* test); at least two independent experiments were performed. **(D and E)** 8-wk-old *Ythdf2*^fl/fl;*Mx1-Cre* (*Ythdf2*^iCKO) and control *Ythdf2*^fl/fl (*Ythdf2*^CTL) mice were treated with six sequential doses of plpC (every other day) to induce deletion of *Ythdf2*. BM LSK CD48⁻CD150⁺ CD45.2⁺ HSCs were sorted from 34-wk-old (D) and 60-wk-old (E) *Ythdf2*^CTL and *Ythdf2*^iCKO mice (as described in Fig. 3 H) before transplantation into lethally irradiated syngeneic CD45.1⁺/CD45.2⁺ recipient mice together with 2 × 10⁵ competitor CD45.1⁺ BM cells. The frequency of B cells, T cells, granulocytes, and monocytes in the CD45.2⁺ compartment of PB, BM, and spleen of recipient mice was analyzed 16 wk after transplantation. Analysis of the percentage of CD45.2⁺ cells in lineage and stem cell compartments is presented in Fig. 3, I–L (*n* = 12). Data represents mean ± SEM; *, P < 0.05; **, P < 0.01; ***, P < 0.001; ****, P < 0.0001 (Mann–Whitney *U* test); at least two independent experiments were performed.

A

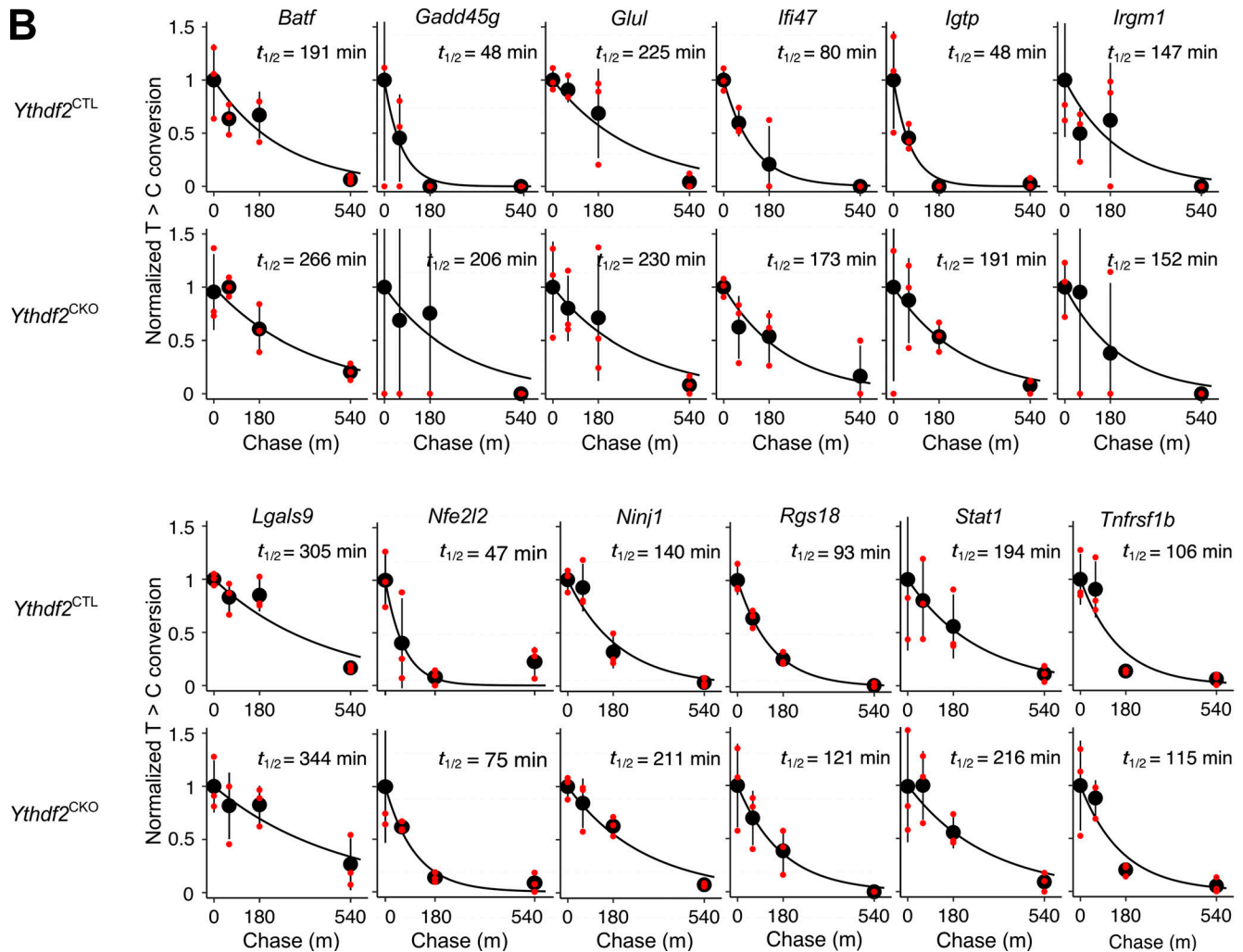| Upstream activator	Activation state	Transcriptome		Proteome	
		Z-Score	P-value of overlap	Z-Score	P-value of overlap
STAT1	Activated	3.17	9.62 E-11	3.266	0.00113
IFN-gamma	Activated	3.013	1.05 E-18	3.864	0.00000098
IRF7	Activated	2.917	9.57 E-08	4.245	1.46 E-08
TLR4	Activated	2.736	2.59 E-07	-	-
TNF-alpha	Activated	2.457	2.51 E-07	2.618	0.0000525
IFNAR	Activated	2.392	4.42 E-06	3.451	6.43 E-11

B

Figure S2. **Molecular properties of HSCs lacking *Ythdf2*. (A)** IPA of RNA-seq and mass spectroscopy from *Ythdf2*[CTL] and *Ythdf2*[CKO] HSCs or c-Kit^{+} cells, respectively. Z-score represents the degree of activation of the pathway, with a threshold for significance set at 2. P value shown refers to the overlap between target genes or proteins in the dataset and target genes in the IPA database. RNA-seq, $n = 4$; proteomics, $n = 5$. **(B)** Decay curves for transcripts in *Ythdf2*[CTL] (upper panels) and *Ythdf2*[CKO] (lower panels) c-Kit^{+} cells are shown. The center value and the error bars at each time point indicate the conversion rate mean and SD, respectively. Conversion rates for each biological replicate are indicated with dots. The half-life for each graph is also shown.
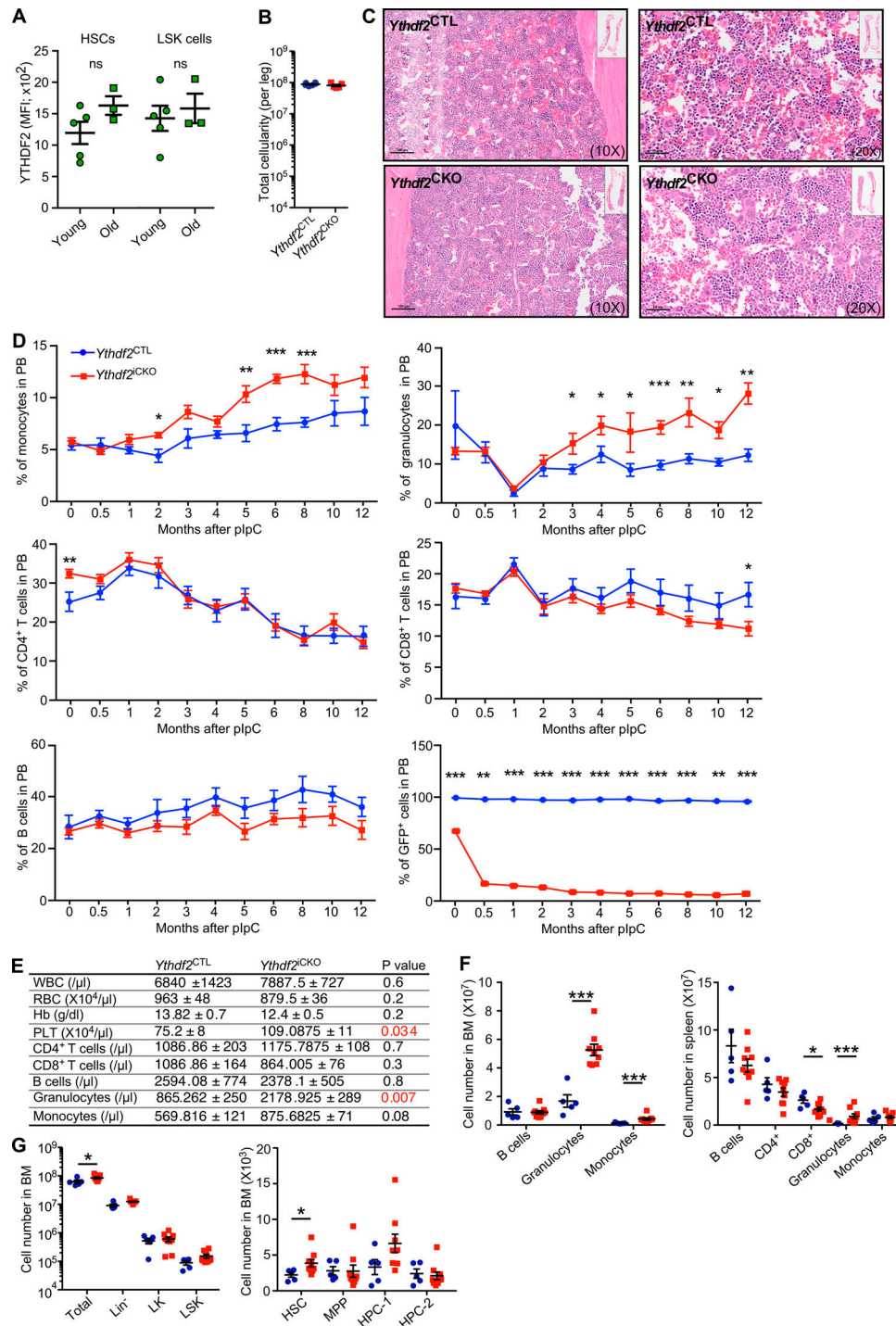
Figure S3. **Inducible deletion of *Ythdf2* from adult mice does not derail long-term steady-state hematopoiesis but results in a progressive myeloid bias and HSC failure upon aging. (A)** Modal YTHDF2-GFP fluorescence assayed by flow cytometry in LSKs and LSK CD48⁻CD150⁺ HSCs from 8–12-wk-old and 60–65-wk-old *Ythdf2*CTL mice. Data represent mean ± SEM; ns, not significant (Mann–Whitney *U* test); at least two independent experiments were performed. **(B)** Total BM cellularity of one leg from 60–65-wk-old *Ythdf2*CTL and *Ythdf2*CKO mice (*n* ≥ 5). Data represent mean ± SEM; at least two independent experiments were performed. **(C)** Representative sections of H&E-stained *Ythdf2*CTL and *Ythdf2*CKO BM at 10× and 20× magnification (*n* ≥ 5). **(D)** Percentage of CD19⁺B220⁺ B cells, CD4⁺ T cells, CD8⁺ T cells, CD11b⁺Gr-1⁺ granulocytes, CD11b⁺Gr-1⁻ monocytes, and GFP-YTHDF2⁺ cells in PB of *Ythdf2*iCKO and *Ythdf2*CTL mice over 12 mo after pIpC treatment. Bottom right, loss of expression of GFP-YTHDF2 following pIpC treatment (*n* ≥ 5). Data represents mean ± SEM; *, P < 0.05; **, P < 0.01; ***, P < 0.001 (Mann–Whitney *U* test); at least two independent experiments were performed. **(E)** PB counts of *Ythdf2*CTL and Ythdf2iCKO mice 12 mo after pIpC treatment (*n* = 5–8). Data represent mean ± SEM; P value by Mann–Whitney *U* test; at least two independent experiments were performed. **(F)** Total number of differentiated cell populations in BM and spleens 12 mo after pIpC treatment (*n* = 5–9). Data represent mean ± SEM; *, P < 0.05; ***, P < 0.001 (Mann–Whitney *U* test); at least two independent experiments were performed. **(G)** Total cell numbers of BM primitive cell populations. HSCs, LSK CD48⁻CD150⁺ HSCs; MPP, LSK CD48⁻CD150⁻; HPC-1, LSK CD48⁺CD150⁻, HPC-2 LSK CD48⁺CD150⁺, and LK Lin⁻Sca-1⁻c-Kit⁺ myeloid progenitors 12 mo after pIpC treatment (*n* = 5–9). Data represent mean ± SEM, *, P < 0.05 (Mann–Whitney *U* test); at least two independent experiments were performed.

Mapperley et al.
YTHDF2 suppresses inflammation to sustain HSCs

Journal of Experimental Medicine   S4
https://doi.org/10.1084/jem.20200829